Alexandria Engineering Journal (2017) xxx, xxx–xxx

HOSTED BY

Alexandria University

Alexandria Engineering Journal

www.elsevier.com/locate/aej
www.sciencedirect.com

ORIGINAL ARTICLE

Numerical simulation of oscillating lid driven square cavity

Jagadeesh Varma Indukuri, Ranjith Maniyeri *

Department of Mechanical Engineering, National Institute of Technology Karnataka (NITK), Surathkal, Mangalore 575025, Karnataka, India

Received 29 March 2017; revised 14 July 2017; accepted 27 July 2017

KEYWORDS

Finite volume method;
First order upwind scheme;
Oscillating lid driven cavity;
Simple algorithm

Abstract This paper aim to develop a two-dimensional computational model to study the fluid dynamic behaviour in a square cavity driven by an oscillating lid using staggered grid based finite volume method. Firstly the developed computational model is validated with that of other researcher's results for the case of finite wall motion. Later the numerical simulations are performed for the case of top wall oscillations for various combinations of Reynolds number and frequencies. From these simulations an optimum frequency is chosen and then with the optimum frequency the simulations are carried out to explore the vortex behaviour for the cases of parallel wall oscillations (both top and bottom walls moving in the same direction) and anti-parallel wall oscillations (both top and bottom walls moving in the opposite direction). From these simulations it may be concluded that $Re = 1000$ is medium range of operation for better mixing inside the cavity for the cases of parallel and anti-parallel wall oscillations.

1. Introduction

Flow in a cavity driven by finite wall motion has long been considered as the benchmark problem in the field of computational fluid dynamics. Eventhough the geometry appears to be simple, but this model provides a better understanding of more complex flow regimes in a cavity. Generally fluid mixing is the important field of research in chemical and process engineering industries. There are several methods involved to enhance the fluid mixing, some methods are like using the stirrers in the flow domain and repeated stretching and folding of the fluid. Oscillating lid improves the disturbances of fluid flow patterns inside the cavity apart from the lid moving with finite wall motion.

Koseff et al. [1] and other researchers have done experimental investigations on end wall effects in lid driven cavity flows [1,2]. Benchmark results are done by Ghia et al. [3] on two-dimensional lid driven square cavity problem for high Reynolds number using a multigrid method. Later the research has been extended to study the effects of aspect ratios on cavity and vortex behaviour inside the cavity for wide range of Reynolds number using lattice Boltzmann method, finite difference method and stream vorticity approach [4–6]. Many studies have been reported on finite wall motions for different configurations of the lid driven cavity for wide range of Reynolds number but, less attention has been made on oscillating lid driven cavity flows with finite volume method. Mendu et al. [7]

* Corresponding author.
E-mail address: mranji1@nitk.edu.in (R. Maniyeri).
Peer review under responsibility of Faculty of Engineering, Alexandria University.

http://dx.doi.org/10.1016/j.aej.2017.07.011

Nomenclature

$\mathbf{u}^*$	X-component of velocity (m/s)
$\mathbf{u}^*_{\mathbf{ref}}$	reference velocity (m/s)
L_c	reference length (m)
U	non-dimensional x-component velocity
$\mathbf{v}^*$	Y-component of velocity (m/s)
V	non-dimensional y-component velocity
p^*	pressure (N/m^2)
P	non-dimensional pressure
Re	Reynolds number

Greek symbols

ρ	density (kg/m^3)
μ	dynamic viscosity ($N\ sec/m^2$)
τ	non-dimensional time
ω^*	natural frequency (radians/s)
ω	non-dimensional frequency

have done the numerical simulations on fluid flow in a cavity driven by an oscillating lid using lattice Boltzmann method. The investigations, mainly focuses on mixing characteristics inside the cavity based on the Reynolds number and the frequency of the lid motion. Zhenhong et al. [8] have investigated the fluid dynamic behaviour in a oscillating lid driven cavity by smoothed hydrodynamic particle approach, where the investigations mainly focusses on low Reynolds number. Sheremat et al. [9] have done numerical study on buoyancy effects in a lid driven cavity filled with a water based nano fluid using stream function and vorticity based formulation. Their investigations helped to know the parameters (moving parameters and Richardson number) that effect the flow, heat and mass transfer mechanisms inside the cavity. Gibanov et al. [10] have presented the mixed convection heat transfer taking place in a lid driven cavity with heat conducting solid backward step. They mainly concentrated on the parameters like Richardson number, distance between the left wall and backward step, nano particle volume fraction, backward step height and thermal conductivity ratio. They mainly concluded that the average Nusselt number near the hot moving lid and nanofluid flow rate are desending functions of backward step height ratio and Richardson number.

Most of the investigations based on the literature survey infers that, wide range of computational study has been carried out using finite wall motions with different configurations. The study on oscillating lid driven cavity has given less attention. Mainly the research on oscillating lid driven cavity has been carried out for the case of single wall oscillation with Reynolds number ranging to 1000 using lattice Boltzmann method and smoothed hydrodynamic particle approach. To the best of our knowledge no investigations have been reported for the cases of parallel and anti-parallel wall oscillations. Motivated by this, we develop a two-dimensional computational model using staggered grid based finite volume method with SIMPLE algorithm [11] to study fluid dynamics of a single wall oscillating lid driven square cavity. Based on the optimum frequency obtained from the simulations of single wall oscillating lid driven square cavity, the simulations are carried out for the cases of parallel wall and anti-parallel wall oscillations with Reynolds number ranging up to 2000.

2. Mathematical modelling and numerical procedure

Fig. 1 shows the schematic diagrams of oscillating lid driven square cavity with different wall oscillation configurations. Fig. 1(a) shows single wall oscillation which is given a horizontal oscillating motion varying as cosine function i.e., $u_{ref}\cos(\omega^* t)$ where u_{ref} is the oscillation amplitude, ω^* is the

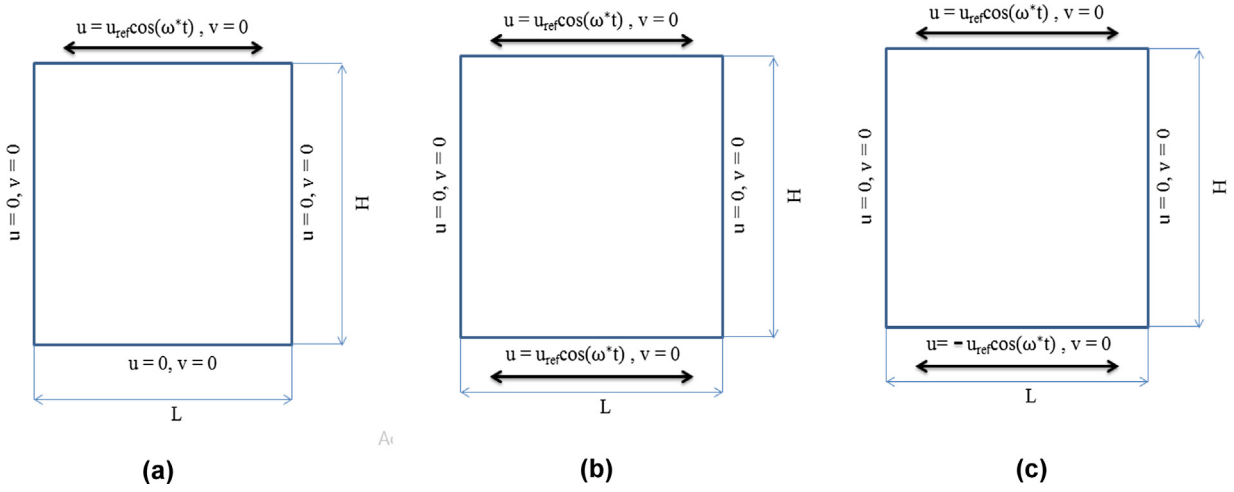

Fig. 1 Schematic diagram representing the physical domain of oscillating lid driven square cavity (a) Single wall oscillation. (b) Parallel wall oscillation and (c) anti-parallel wall oscillation.

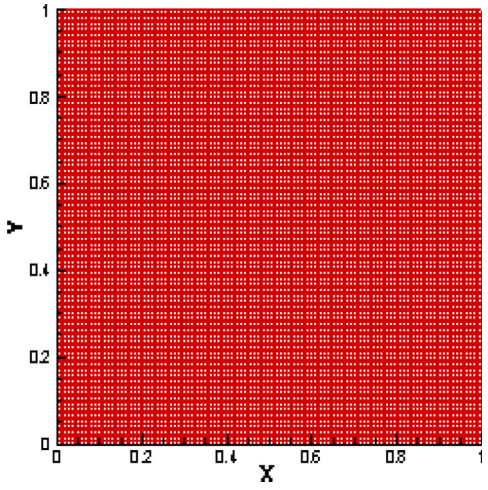

Fig. 2 Schematic diagram representing the grid size 129 × 129.

Table 1 Dimensional boundary conditions for oscillating wall cases.

Walls	Single wall oscillation	Parallel wall oscillation	Anti-parallel oscillation
Top wall	$u^* = u^*_{ref}\cos(\omega^* t^*)$, $v^* = 0$, $y^* = H$, $0 \le x^* \le L$	$u^* = u^*_{ref}\cos(\omega^* t^*)$, $v^* = 0$, $y^* = H$, $0 \le x^* \le L$	$u^* = u^*_{ref}\cos(\omega^* t^*)$, $v^* = 0$, $y^* = H$, $0 \le x^* \le L$
Bottom wall	$u^* = v^* = 0$, $y^* = 0$, $0 \le x^* \le L$	$u^* = u^*_{ref}\cos(\omega^* t^*)$, $v^* = 0$, $y^* = 0$, $0 \le x^* \le L$	$u^* = -u^*_{ref}\cos(\omega^* t^*)$, $v^* = 0$, $y^* = 0$, $0 \le x^* \le L$
Left wall	$u^* = v^* = 0$, $x^* = 0$, $0 \le y^* \le H$	$u^* = v^* = 0$, $x^* = 0$, $0 \le y^* \le H$	$u^* = v^* = 0$, $x^* = 0$, $0 \le y^* \le H$
Right wall	$u^* = v^* = 0$, $x^* = L$, $0 \le y^* \le H$	$u^* = v^* = 0$, $x^* = L$, $0 \le y^* \le H$	$u^* = v^* = 0$, $x^* = L$, $0 \le y^* \le H$

oscillating frequency and t is the time period of oscillation. Fig. 1(b) shows parallel wall oscillation in which both top and bottom walls moving with same oscillating velocity and Fig. 1(c) represents anti-parallel wall oscillation in which both top and bottom wall are given opposite oscillations.

We use a uniform grid system comprising of 129 × 129 grid which is shown in Fig. 2. The selected grid size is optimum one based on grid independent test.

The flow behaviour inside the cavity is studied using continuity and Navier-Stokes equations, which are shown below in Eqs. (1) and (2) in dimensional form as,

$$\nabla \cdot \mathbf{u}^* = 0 \tag{1}$$

$$\rho\left(\frac{\partial \mathbf{u}^*}{\partial t^*} + \mathbf{u}^* \cdot \nabla \mathbf{u}^*\right) = -\nabla p^* + \mu \nabla^2 \mathbf{u}^* \tag{2}$$

The dimensional boundary conditions for the case of single wall, parallel wall and anti-parallel wall oscillation case is shown in Table 1.

Table 2 Non-dimensional boundary conditions for oscillating wall cases.

Walls	Single wall oscillation	Parallel wall oscillation	Anti-parallel oscillation
Top wall	U = cos (ωτ), V = 0, Y = 1.0, 0 ≤ X ≤ 1.0	U = cos (ωτ), V = 0, Y = 1.0, 0 ≤ X ≤ 1.0	U = cos (ωτ), V = 0 Y = 1.0, 0 ≤ X ≤ 1.0
Bottom wall	U = V = 0, Y = 0, 0 ≤ X ≤ 1.0	U = cos (ωτ), V = 0, Y = 0, 0 ≤ X ≤ 1.0	U = −cos (ωτ), V = 0, Y = 0, 0 ≤ X ≤ 1.0
Left wall	U = V = 0, X = 0, 0 ≤ Y≤1.0	U = V = 0, X = 0, 0 ≤ Y ≤ 1.0	U = V = 0, X = 0, 0 ≤ Y ≤ 1.0
Right wall	U = V = 0, X = 1.0, 0 ≤ Y ≤ 1.0	U = V = 0, X = 1.0, 0 ≤ Y≤1.0	U = V = 0, X = 1.0, 0 ≤ Y ≤ 1.0

The geometric and flow variables in the continuity and momentum equations are non-dimensionalised using characteristic values of length, velocity and time as shown below. $U = \frac{u^*}{u^*_{ref}}$, $V = \frac{v^*}{u^*_{ref}}$, $X = \frac{x^*}{L_c}$, $Y = \frac{y^*}{L_c}$, $\omega = \frac{\omega^* L_c}{u^*_{ref}}$, $P = \frac{P^*}{\rho u^{*2}_{ref}}$, $\tau = \frac{t^* u^*_{ref}}{L_c}$, where 'ref' means characteristic values.

The non-dimensionalized continuity and momentum equations are shown below in Eqs. (3) and (4).

$$\nabla \cdot \mathbf{U} = 0 \tag{3}$$

$$\left(\frac{\partial \mathbf{U}}{\partial \tau} + \mathbf{U} \cdot \nabla \mathbf{U}\right) = -\nabla P + \frac{1}{Re}\nabla^2 \mathbf{U} \tag{4}$$

where Re is called Reynolds which is given as $Re = \frac{\rho u_{ref} L_c}{\mu}$. The non-dimensional boundary conditions for oscillating wall cases are given in Table 2.

In this present work staggered grid based finite volume method is used with SIMPLE algorithm [11] to solve the

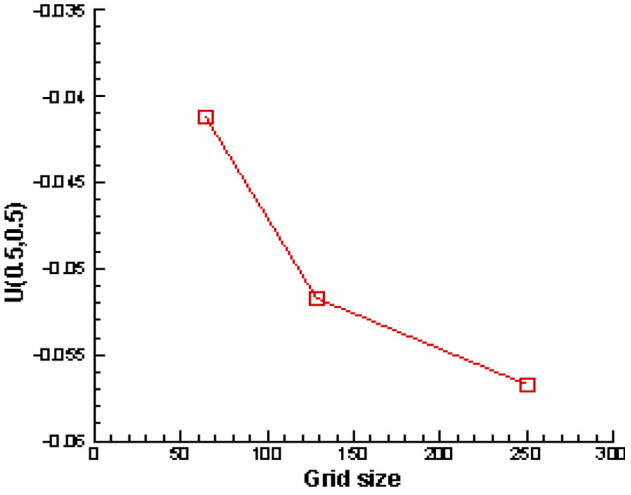

Fig. 3 Schematic diagram representing grid independence test (65 × 65, 129 × 129, 251 × 251) for mid-point x component velocity for the case of finite wall motion at Re = 1000.

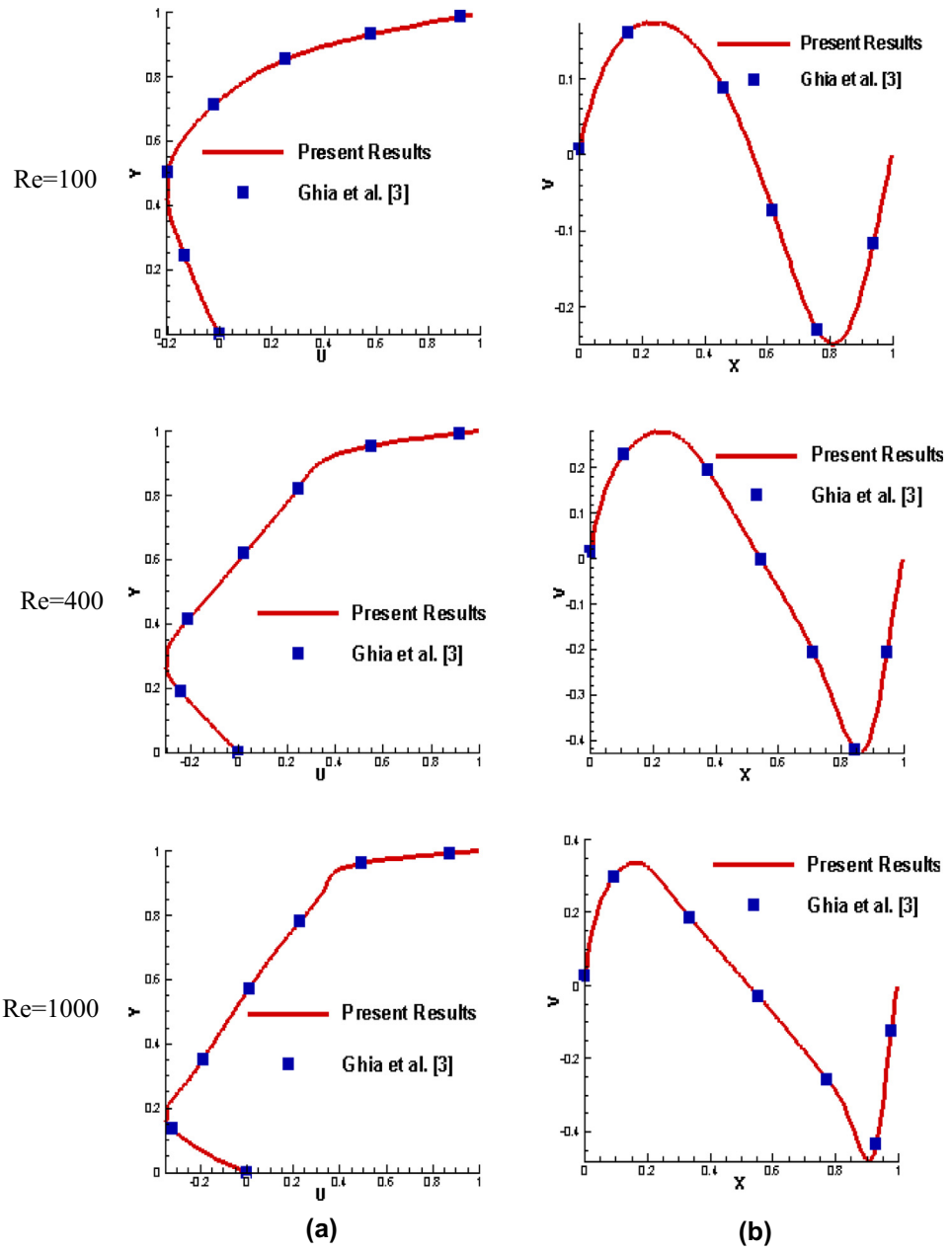

Fig. 4 Validation of present results for finite wall motion (a) Centerline u velocity variation along y axis. (b) Centerline v velocity variation along x axis.

continuity and momentum equations. The convective terms in the momentum equations are treated with first order upwind scheme and the algebraic equations obtained for X and Y momentum equations are solved using TDMA (tridiagonal matrix algorithm). Euclidean norm of residual is taken into consideration for convergence of each independent flow variable.

The discretised form of convective fluxes at the east, west, north and south faces are represented below

$$F_e = ((u_{i,j} + u_{i+1,j}) * dy)/2.0$$

$$F_w = ((u_{i,j} + u_{i-1,j}) * dy)/2.0$$

$$F_n = ((v_{i,j} + v_{i+1,j}) * dx)/2.0$$

$$F_s = ((v_{i,j-1} + v_{i+1,j-1}) * dx)/2.0$$

where $u_{i,j}$ and $v_{i,j}$ are x-direction and y-direction velocities, dx and dy are grid sizes in x and y direction. The discretisation form of diffusion terms at east, west, north and south faces are calculated by the following terms given below,

$$D_e = \frac{dy}{(Re * dx)}, \quad D_w = \frac{dy}{(Re * dx)}, \quad D_n = \frac{dx}{(Re * dy)},$$

$$D_s = \frac{dx}{(Re * dy)}$$

Please cite this article in press as: J.V. Indukuri, R. Maniyeri, Numerical simulation of oscillating lid driven square cavity, Alexandria Eng. J. (2017), http://dx.doi.org/10.1016/j.aej.2017.07.011

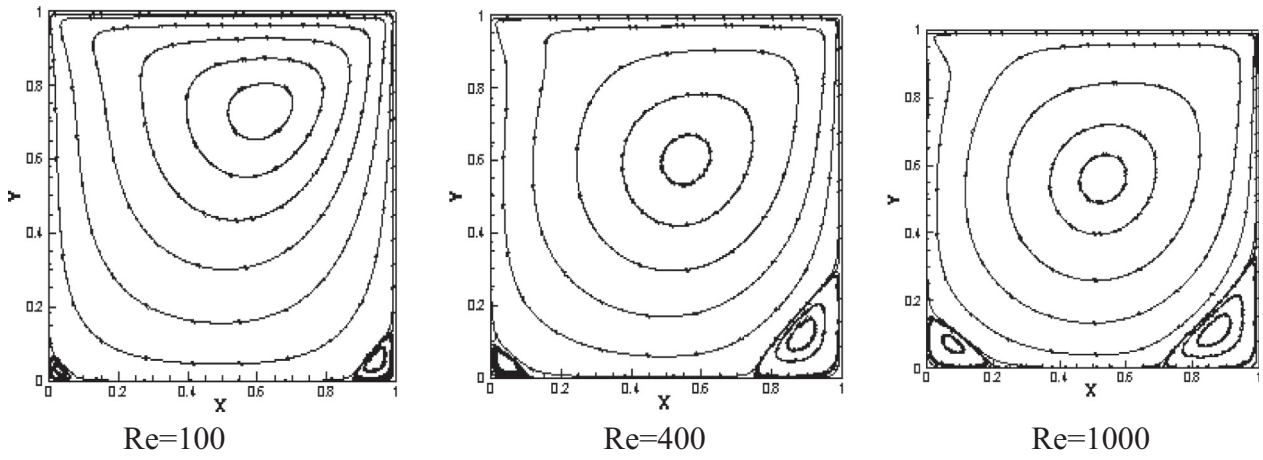

Fig. 5 Schematic diagrams representing the streamline patterns for the case of top wall motion for a range of Reynolds number.

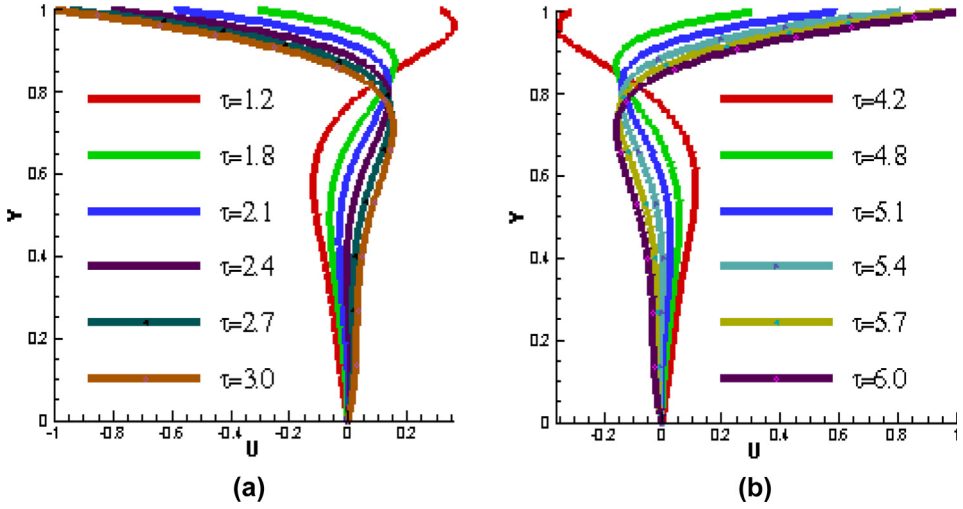

Fig. 6 . Centerline u and v velocity variation for single wall oscillation $Re = 100$ and $\omega = 2\pi/6$ (a) first half cycle ($\tau = 0$–3). (b) Second half cycle ($\tau = 3$–$\tau = 6$).

The convergence term is taken into account after solving the momentum equations for the case of steady state problem which is represented in Eq. (5), whereas for the unsteady state problem like oscillating lid driven cavity no convergence is taken into consideration, but it is ensured that the solution is oscillatory after certain time periods and then the results are captured at certain time step.

$$(u_{i,j} - u_{i-1,j})\Delta y + (v_{i,j} - v_{i,j-1})\Delta x \leqslant 10^{-8} \quad (5)$$

3. Results and discussions

3.1. Grid independence test

The grid independence test is done for the case of standard lid driven square cavity with top wall moving with finite motion having Reynolds number case ($Re = 1000$) and the remaining walls are kept at stationary position. Mainly, the grid independent test is done for three different uniform grid sizes of 65×65, 129×129 and 251×251. The variation of the mid-point x component velocity is taken into consideration for different grid sizes. Fig. 3 represents the variation of mid-point velocity for different grid sizes. From Fig. 3 it is observed that the solution accuracy is nearly same for the case of 129×129 and 251×251 with a deviation of only 5%. Since, the grid size 251×251, takes large computational time to get the same results, we chose 129×129 as the optimum grid size for further simulations. It is to be noted that, Ghia et al. [3] have used the same grid size 129×129 with whom the validation of the present work is done for different Reynolds numbers.

3.2. Validation of the developed model

First of all, the developed numerical model for a square cavity of size 1×1 is used to validate for the case of single wall

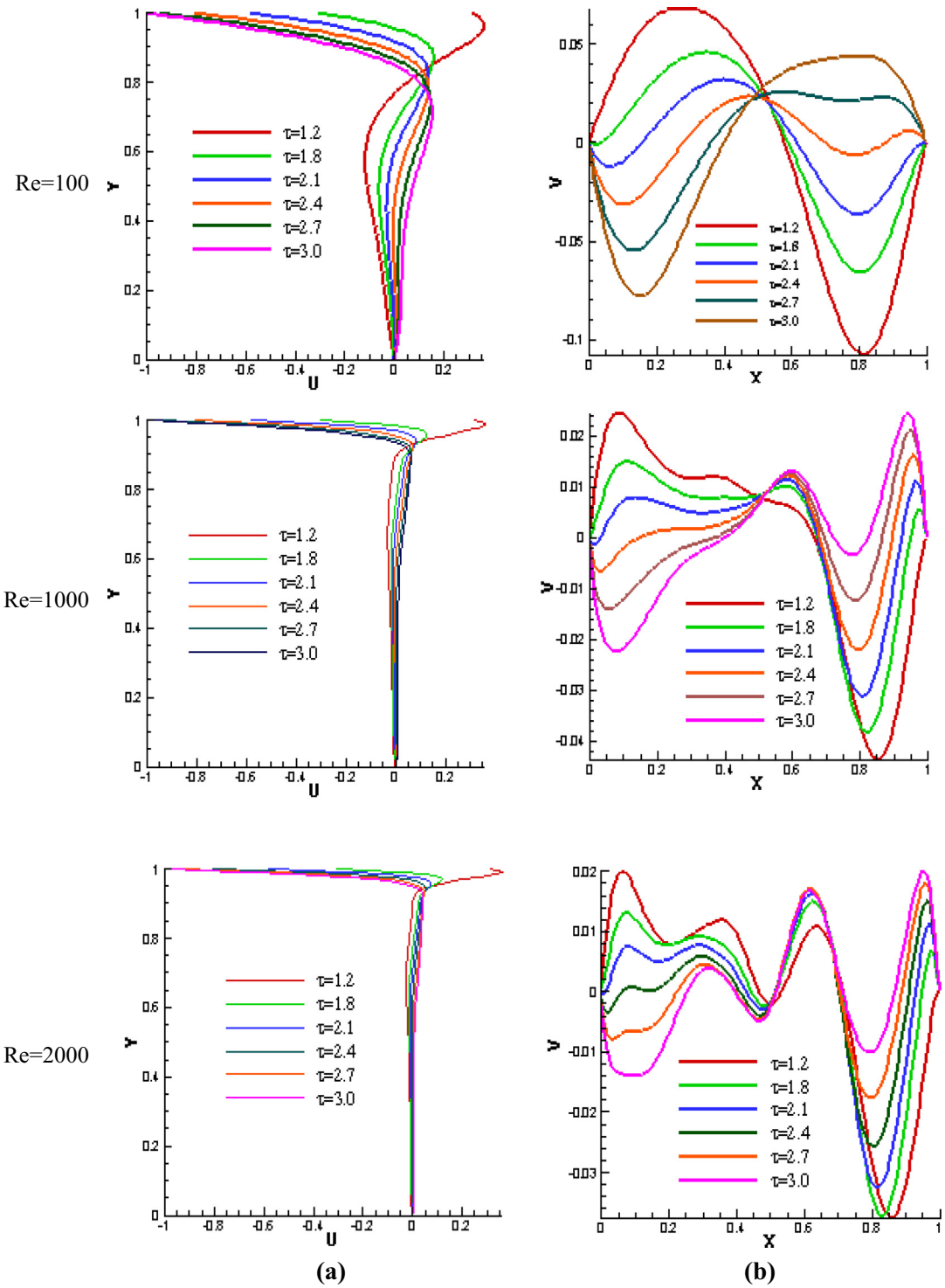

Fig. 7 Centerline velocity variation for single wall oscillation for range of Reynolds number and ω = 2π/6 first half cycle (τ = 0–3.0) (a) u velocity variation along y axis. (b) v velocity variation along x axis.

motion (top wall moving with finite velocity) for three different Reynolds numbers (*Re* = 100, 400 and 1000). We select a time step of 0.01. Fig. 4(a) and (b) shows the comparison of present results of u and v velocity variation along y and x axis at the centre of the cavity with that of Ghia et al. [3] results. From these plots, it can be seen that the present results are in good agreement with that of Ghia et al. [3] which proves the reliability of our developed model. Fig. 5 shows the streamline patterns inside the cavity for the three Reynolds numbers for top wall motion. From Fig. 5 it can be inferred that, as the

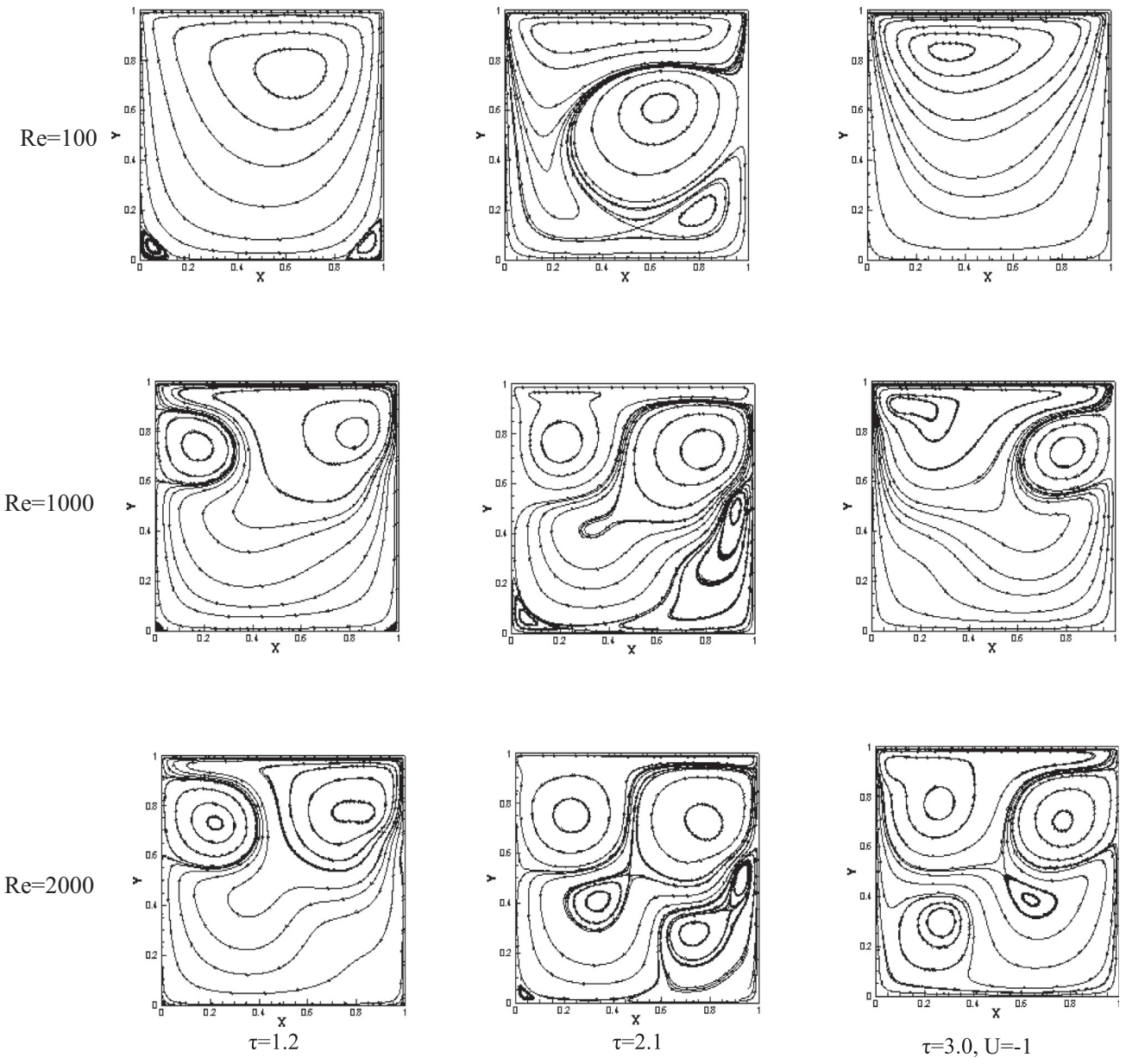

Fig. 8 Streamline patterns for single wall oscillation at various time intervals with optimum frequency ω = 2π/6.

Reynolds number increases, the formation of primary vortex center moves towards the geometric center and the increase in size of secondary corner vortices is also noticed.

3.3. Single wall oscillation

Next, simulations are performed with the developed model for single wall oscillation. The numerical simulations are performed for various Reynolds number ranging from *Re* = 100 to 2000 with various frequency's $\left(\omega = \frac{\pi}{6}, \frac{2\pi}{6}, \frac{5\pi}{6}, \pi, \frac{4\pi}{3}\right)$ and 2π. For every frequency there are certain periodic oscillations. Based on the frequency of oscillation certain time step is decided to capture the fluid behaviour inside the cavity. By observing how well the lid oscillations are transferred to bulk motion of the fluid inside the cavity for various frequencies, an optimum frequency is chosen as $\omega = \frac{2\pi}{6}$. Fig. 6(a) shows the variation of centerline u velocity along y axis for the first half cycle τ = 0–3). From this figure an interesting fluid behaviour is observed when compared to that of lid moving with a finite velocity case in Fig. 4(a). Here, the x component of fluid velocity from top to bottom experiences more complex behaviour than the case of lid moving with finite velocity. This phenomenon is happening mainly due to the oscillatory motion of lid. Similarly, Fig. 6(b) shows the centerline u velocity variation for the second half cycle τ = 3.0–6.0), which clearly indicates u velocity variation is exactly reversal of the first half cycle and conforms the periodicity.

Fig. 7 indicates the centre line u velocity variation along the ordinate and v velocity variation along the abscissa for singe oscillating wall case. From Fig. 7(a) it is observed that initially

Please cite this article in press as: J.V. Indukuri, R. Maniyeri, Numerical simulation of oscillating lid driven square cavity, Alexandria Eng. J. (2017), http://dx.doi.org/10.1016/j.aej.2017.07.011

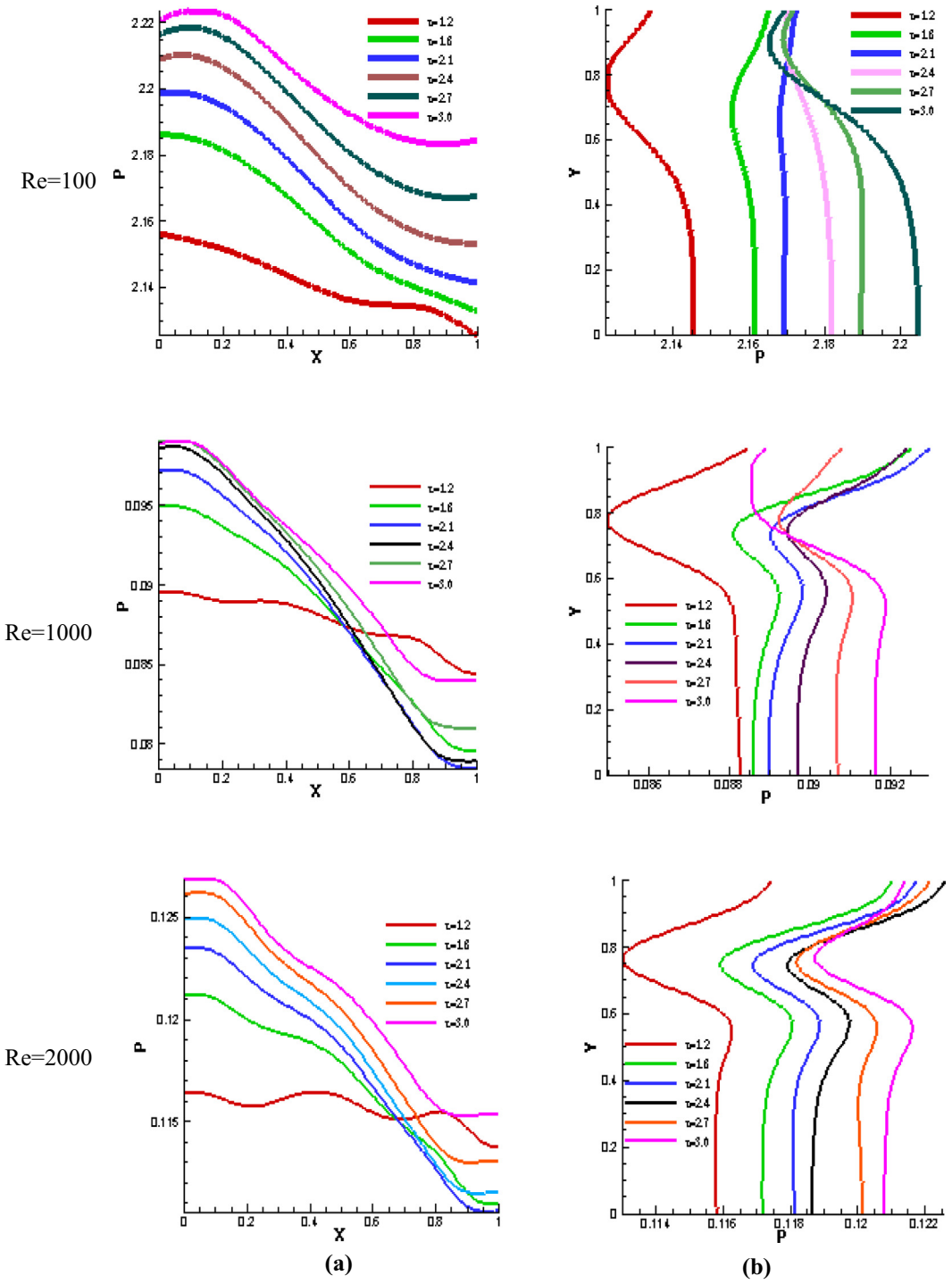

Fig. 9 Pressure distribution for single wall oscillation at first half time interval (τ = 0–3.0) with optimum frequency $\omega = 2\pi/6$ (a) Center line pressure variation along abscissa. (b) Center line pressure variation along ordinate.

at low Reynolds number the particles near to lid portion experiences higher disturbances, as the Reynolds number increases the disturbances are restricted near to the lid portion. From Fig. 7(b) it is observed that for low Reynolds number (Re = 100) case two local maxima values can be found for a particular time step. This maxima value indicates the presence of two vortices inside the cavity (Primary and counter rotating vortex). As the Reynolds number increases (Re = 1000, 2000) local maxima values (four) increases indicating that presence of more complex vortices inside the cavity.

Fig. 8 shows the streamline patterns for the case of single wall oscillation with Reynolds number ranging from 100 to 2000 for optimum frequency ($\omega = \frac{2\pi}{6}$). From Fig. 8, for Re = 100 at time τ = 1.2, it is observed that the major portion

Please cite this article in press as: J.V. Indukuri, R. Maniyeri, Numerical simulation of oscillating lid driven square cavity, Alexandria Eng. J. (2017), http://dx.doi.org/10.1016/j.aej.2017.07.011

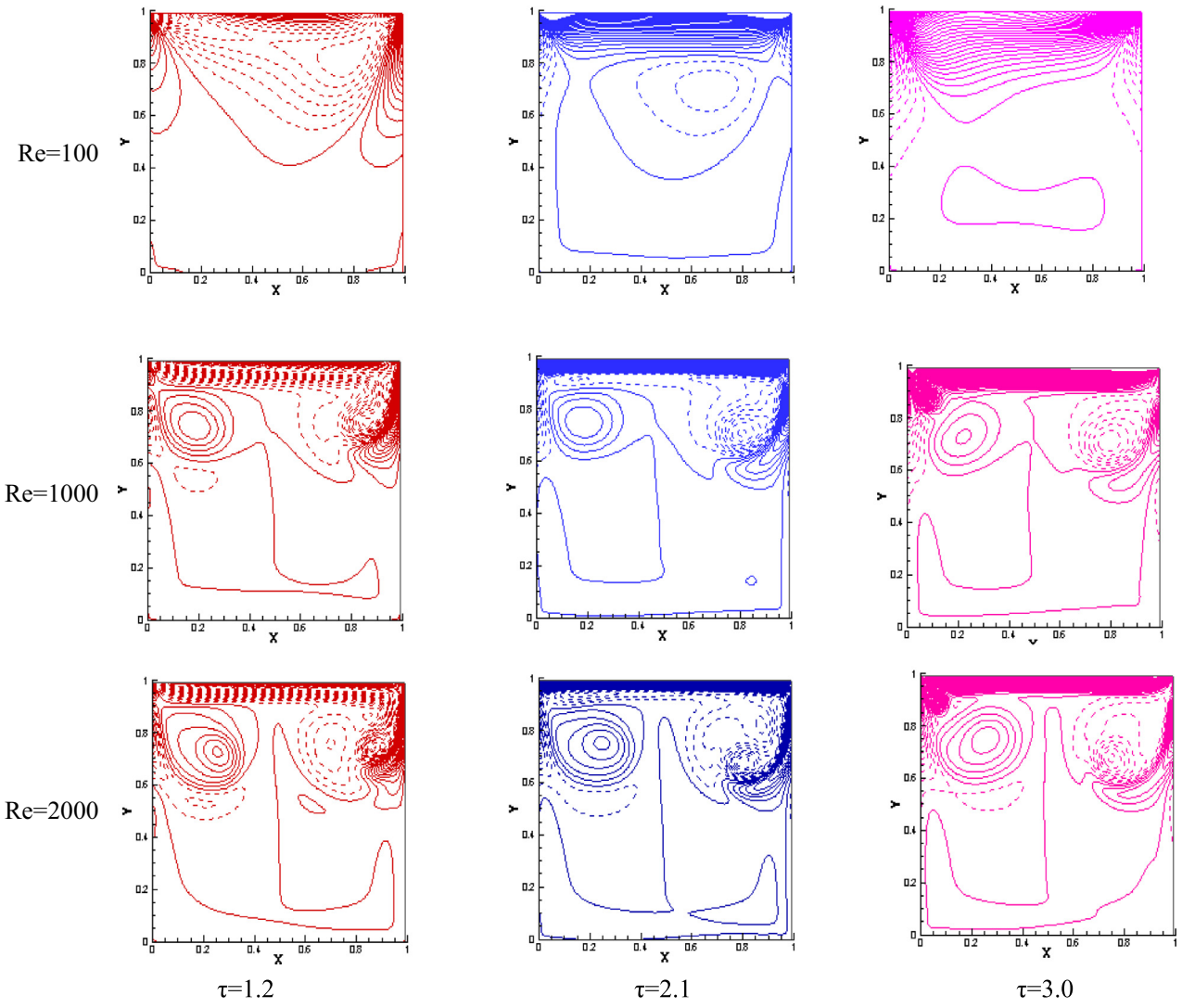

Fig. 10 Vorticity contours for single wall oscillation at various time intervals with optimum frequency $\omega = 2\pi/6$.

of the cavity is filled by the primary vortex and minor portion is occupied by the secondary vortices at the corners, which is interesting that the behaviour is almost same as that of lid moving with finite velocity at the same Reynolds number. At time $\tau = 2.1$ as the lid reverses its direction ($U = -0.58778$) a counter rotating vortex is observed just below the lid and the counter rotating vortex penetration is restricted by primary vortex. Finally, as the time progresses at the end of simulations at $\tau = 3.0$ the entire cavity is dominated by secondary vortex by completely mixing with the primary vortex. For $Re = 1000$ and $\tau = 1.2$ it is interesting to note that along with the primary vortex a secondary vortex is formed near the left wall. As the time progresses the secondary vortex near the left top corner wall enlarges its size by mixing with the counter rotating vortex generated by the reversal motion of the lid. At time $\tau = 2.1$ two secondary vortices are formed, one at the right side wall and the other is at the left bottom corner. Interestingly, the primary vortex is diminished along the diagonal side in case of $Re = 1000$. Finally, at the first half time interval, the most of the space inside the cavity is dominated by a secondary vortex leaving the primary vortex at the top right corner of the cavity. For $Re = 2000$ the behaviour of streamline patterns are almost same for the similar instantaneous lid velocity, only change can be inferred that, at the maximum reversal lid velocity ($U = -1.0$) the size of the primary vortex at the top right corner is more when compared to the case of $Re = 1000$.

Fig. 9 shows the center line pressure along x direction and the center line pressure along y direction for first half time interval single wall oscillation ($\tau = 0$–3.0). From Fig. 9(a) it is observed that at intially time period $\tau = 1.2$) the pressure magnitude inside the cavity is low, as the time period $\tau = 1.8$–3.0) goes on increasing the pressure magnitude goes high. The magnitude of pressure is high for low Re ($Re = 100$) cases and also the pressure magnitude is reducing when it is moved along the x axis for all time intervals. As the Re increases ($Re = 1000$) the

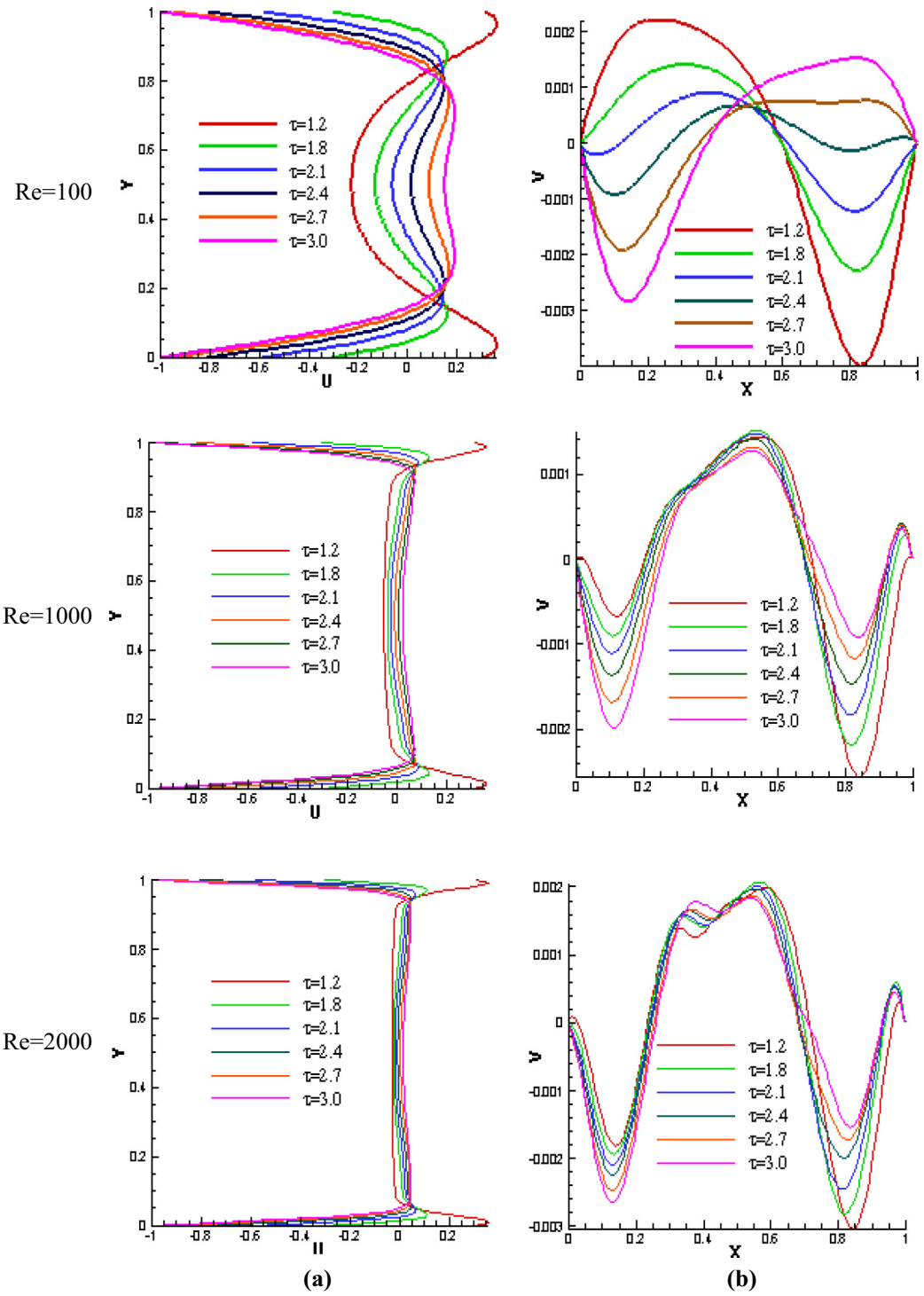

Fig. 11 Centerline velocity variation for parallel wall oscillation for range of Reynolds number and $\omega = 2\pi/6$ first half cycle (τ = 0–3.0) (a) u velocity variation along y axis. (b) v velocity variation along x axis.

pressure magnitude inside the cavity is reducing which can be clearly observed from the plots. From Fig. 9(b) it is observed that the pressure fluctuation along y axis is more near to the top wall for all Reynolds number cases.

The vorticity contours indicated in Fig. 10 shows the distribution of vorticity gradients inside the cavity for a range of Reynolds number. The dark lines indicate positive trend of vorticity and dashed lines as negative trend of vorticity. The vorticity gradients are not high in case of single wall oscillation mainly at the bottom part of the cavity. This indirectly indicates that, the momentum transfer for the case of single wall oscillation is taking place near to the lid.

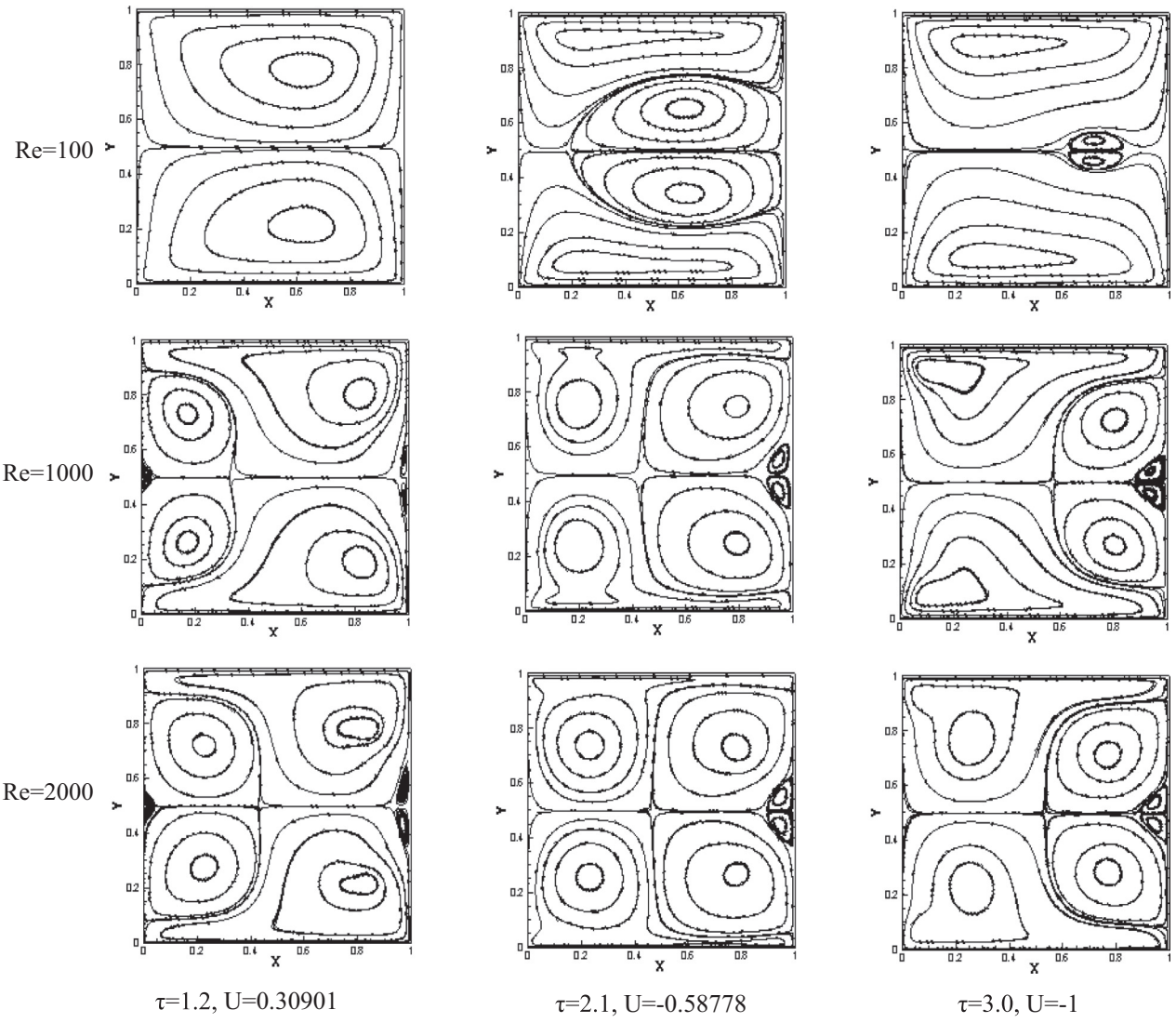

Fig. 12 Streamline patterns for parallel wall oscillation at various time intervals with optimum frequency $\omega = 2\pi/6$.

3.4. Parallel wall oscillation

Fig. 11 shows the centre line u velocity variation along the ordinate and v velocity variation along the abscissa for parallel oscillating wall case. From Fig. 11(a) it is observed that initially at low Reynolds number ($Re = 100$) the particles at the centre part of the cavity experiences higher disturbances, as the Reynolds number increases the disturbances at the centre part of the cavity decreases. From Fig. 11(b) it is observed that for low Reynolds number ($Re = 100$) case two local maxima values can be found for a particular time step. This maxima value indicates the presence of two major vortices inside the cavity (two primary vortices). As the Reynolds number increases ($Re = 1000$, 2000) local maxima values (three) increases indicating the presence of major vortices (primary and counter rotating vortices) occupying the cavity space.

Fig. 12 shows the streamline patterns for the case of parallel wall oscillations, at $Re = 100$, 1000 and 2000 with optimum frequency. From Fig. 12 it is seen that at initial time period $\tau = 1.2$ for the case of $Re = 100$ there are two primary vortices which are mirror images to each other from the centreline of y axis. As the time period is increasing $\tau = 2.1$ the lid reverses its direction creating two counter rotating vortex at the top and bottom part of the cavity by diminishing the primary vortex. Finally, at the first half time period ($\tau = 3.0$), major portion of the cavity is dominated by two counter rotating vortices and minor portion by primary vortices which are mirror images to each other.

For the case of $Re = 1000$, at the initial time period $\tau = 1.2$, along with the primary vortex, a secondary vortex at the left hand side wall is observed, which are also mirror images to each other. As the time period advances $\tau = 1.2$ the two secondary vortices near the left hand side wall increases its size by mixing with the counter rotating vortex, which is formed due to reversal of lid motion at the upper and lower part of the cavity. At the end of first half time

Please cite this article in press as: J.V. Indukuri, R. Maniyeri, Numerical simulation of oscillating lid driven square cavity, Alexandria Eng. J. (2017), http://dx.doi.org/10.1016/j.aej.2017.07.011

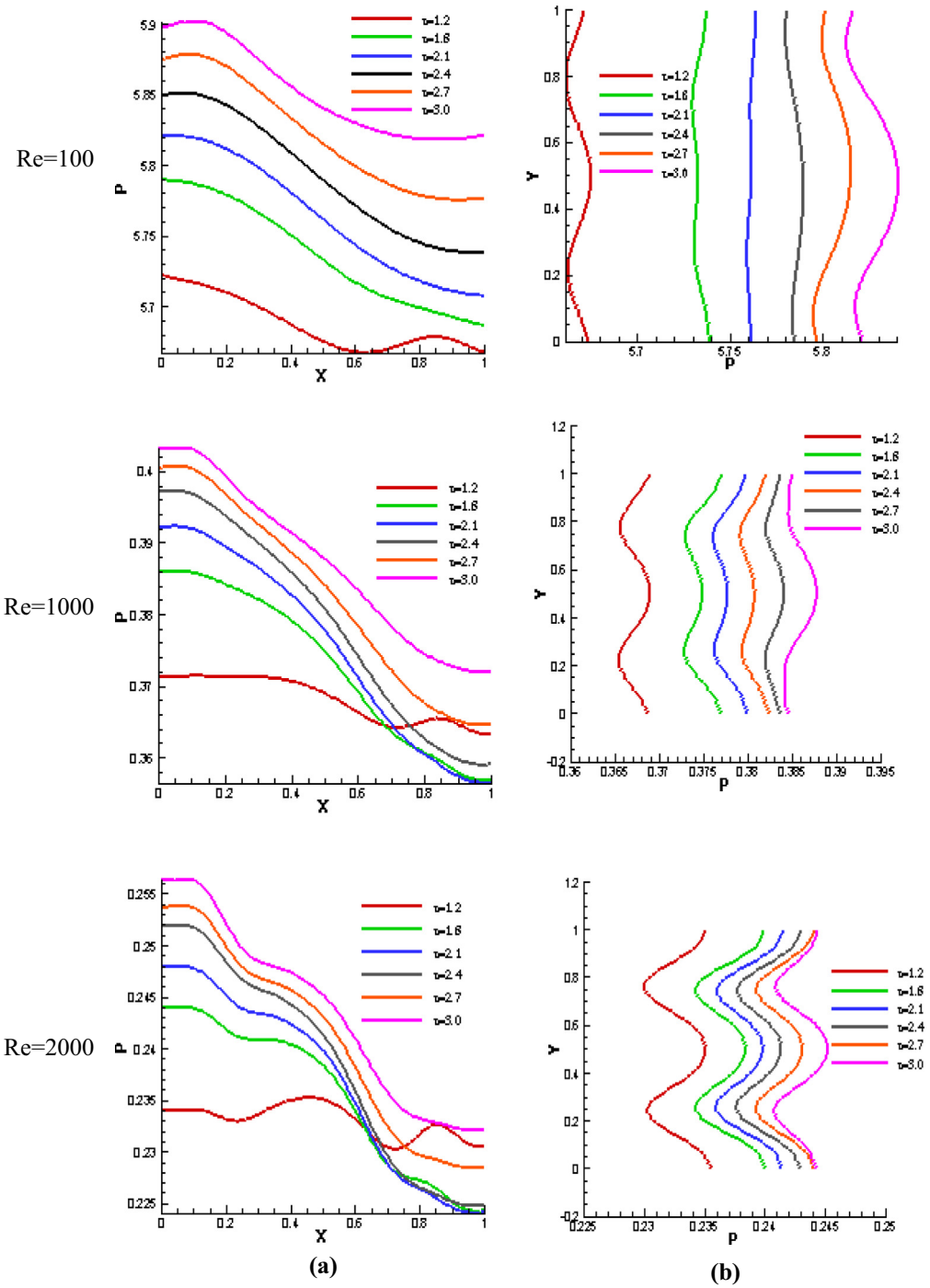

Fig. 13 Pressure distribution for parallel wall oscillation at first half time interval with optimum frequency ω = 2π/6 (a) Center line pressure variation along abscissa. (b) Center line pressure variation along ordinate.

$\tau = 3.0$ the counter rotating vortex in the cavity occupies the main portion of the top and bottom part of the cavity leaving the primary vortices and a small secondary vortices at the right boundary of the cavity. For $Re = 2000$, the streamline patterns behaviour is almost same as that of case $Re = 1000$. The only minor change is that, the size of the primary vortex formed at the right side wall of the cavity at $\tau = 3.0$ is large when compared to the case of $Re = 1000$.

Fig. 13 indicates the center line pressure along x direction and the center line pressure along y direction for first half time interval parallel wall oscillation $\tau = 0$–3.0). From Fig. 13(a) it is observed that the magnitude of pressure is high for low Re ($Re = 100$) cases and also the pressure magnitude is reducing when it is moved along the x axis for all time intervals. The pressure magnitudes in case of parallel wall oscillating case is more when compared to single wall oscillating case which

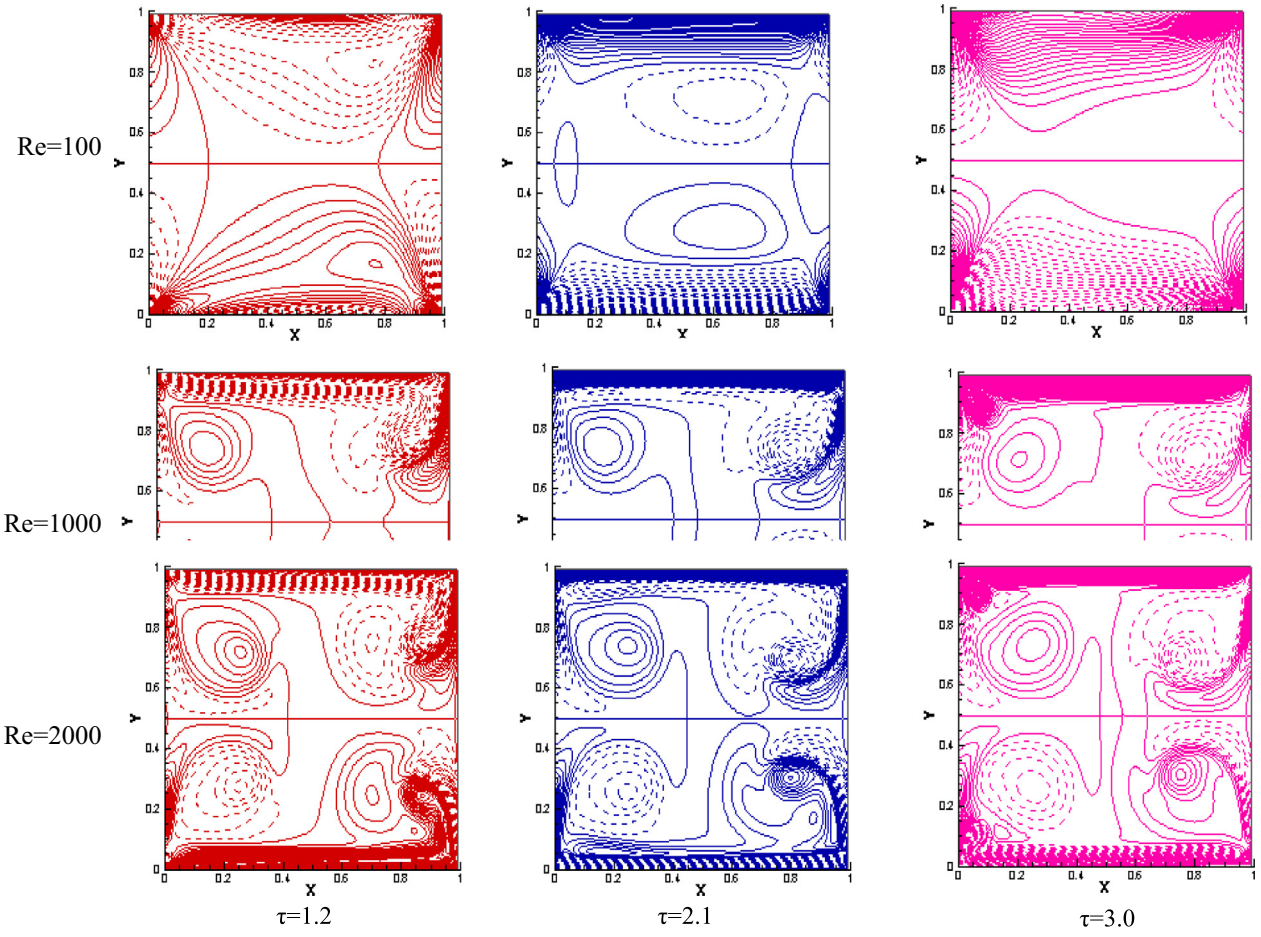

Fig. 14 Vorticity contours for parallel wall oscillation at various time intervals with optimum frequency $\omega = 2\pi/6$.

can clearly observed from the pressure plots. As the *Re* increases ($Re = 1000$) the pressure magnitude inside the cavity is reducing which can be clearly observed from the plots. From Fig. 13(b) it is observed that the pressure fluctuation along y axis is more at the middle portion of the cavity for high Reynolds number ($Re = 1000, 2000$) cases.

Fig. 14 shows the vorticity contours for the case of parallel wall oscillation. The vorticity gradients are high for the cases of high Reynolds number ($Re = 1000, 2000$) when compared to low Reynolds number ($Re = 100$) at different time intervals.

3.5. Anti-parallel wall oscillation

Fig. 15 shows the centre line u velocity variation along the ordinate and v velocity variation along the abscissa for anti-parallel oscillating wall case. From Fig. 15(a) it is observed that initially at low Reynolds number ($Re = 100$) the particles at the centre part of the cavity experiences twisted tape like disturbances indicating the presence of co-rotating vortices, as the Reynolds number increases the disturbances at the centre part of the cavity decreases. From Fig. 15(b) it is observed that for low Reynolds number ($Re = 100$) case two local maxima values can be found for any particular time step. This maxima value indicates the presence of two major vortices inside the cavity (primary and counter rotating vortices). As the Reynolds number increases ($Re = 1000, 2000$) local maxima values (three) increases indicating the presence of at least one vortex at the local maxima (primary or counter rotating vortices) occupying the cavity space.

Fig. 16 shows the streamline patterns for the case of anti-parallel wall oscillation at $Re = 100, 1000$ and 2000 with optimum frequency. In Fig. 16, at initial time period ($\tau = 1.2$) for the case of $Re = 100$, it is can be seen that, a pair of two co-rotating vortices in the main primary vortex. As the time period increases ($\tau = 2.1$) a counter rotating vortex is formed at the upper and lower portion of the cavity detaching the primary vortex. At the first half time period ($\tau = 3.0$) the entire cavity is occupied by counter rotating vortex by mixing with primary vortex. When the Reynolds number increases from 100 to 1000, the streamline pattern behaviour is entirely different when compared to the case of $Re = 100$. At the initial time period ($\tau = 1.2$) a primary vortex aligned diagonally containing two co-rotating vortex and two secondary vortex at the upper left and lower right corners of the cavity is observed. As the time advances ($\tau = 2.1$) the top left and bottom right portion vortices of the cavity tries to mix with counter rotating vortex at the top and bottom part of the cavity which is formed due to the reversal of the lid direction. Finally at the first half

Please cite this article in press as: J.V. Indukuri, R. Maniyeri, Numerical simulation of oscillating lid driven square cavity, Alexandria Eng. J. (2017), http://dx.doi.org/10.1016/j.aej.2017.07.011

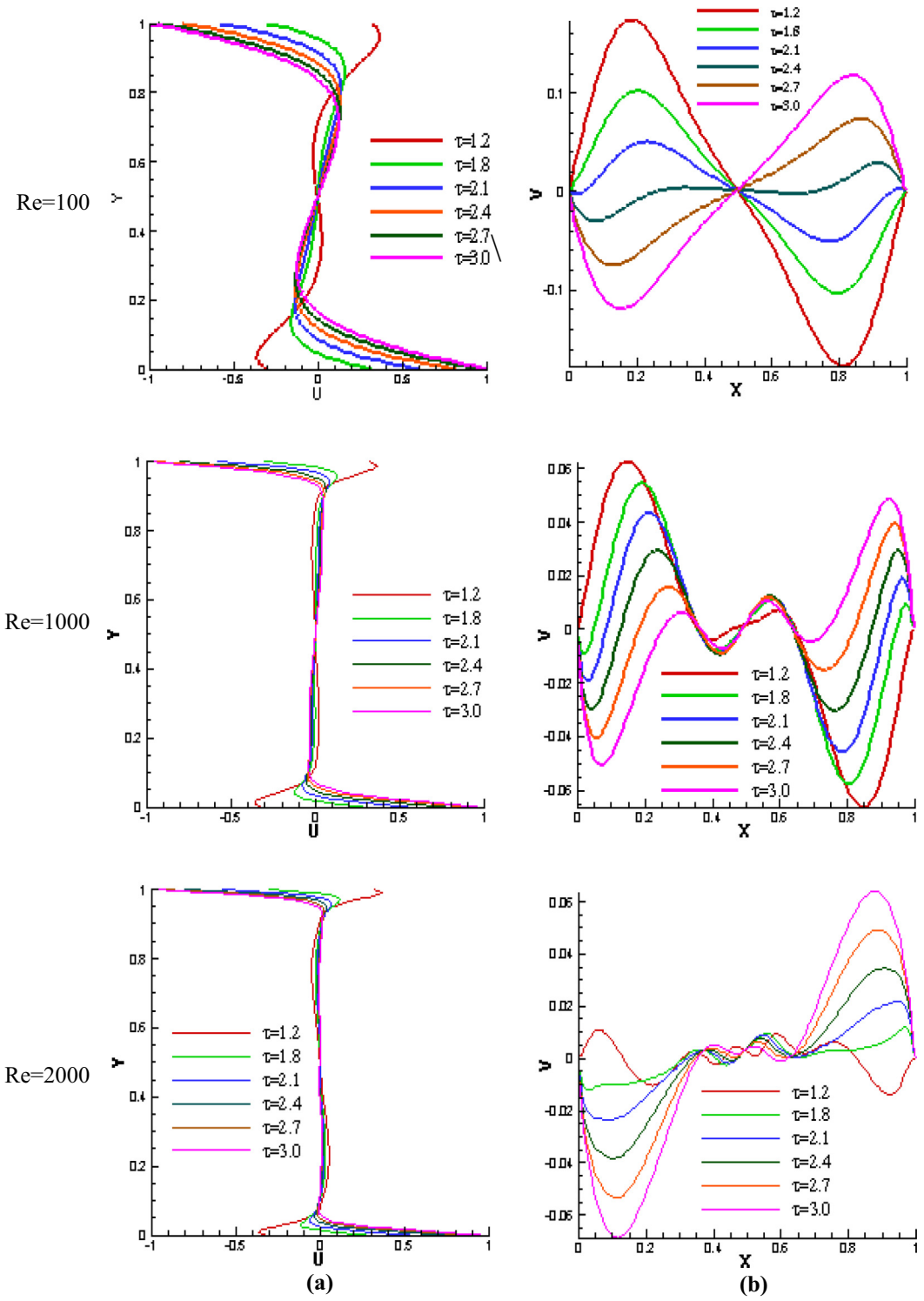

Fig. 15 Centerline velocity variation for anti-parallel wall oscillation for range of Reynolds number and $\omega = 2\pi/6$ first half cycle (τ = 0–3.0) (a) u velocity variation along y axis. (b) v velocity variation along x axis.

time period ($\tau = 3.0$) the entire cavity is occupied by counter rotating vortex leaving primary vortex at the top right and bottom left of the cavity. When the Reynolds number has increased from 1000 to 2000, the streamline patterns behaviour is almost nearly same, but at the final time period ($\tau = 3.0$), the size of the primary vortex formed at the top right and bottom left part of cavity is slightly large in size when compared to that of $Re = 1000$ case.

Fig. 17 indicates the pressure plots at the center line pressure along x direction and center line pressure along y direction

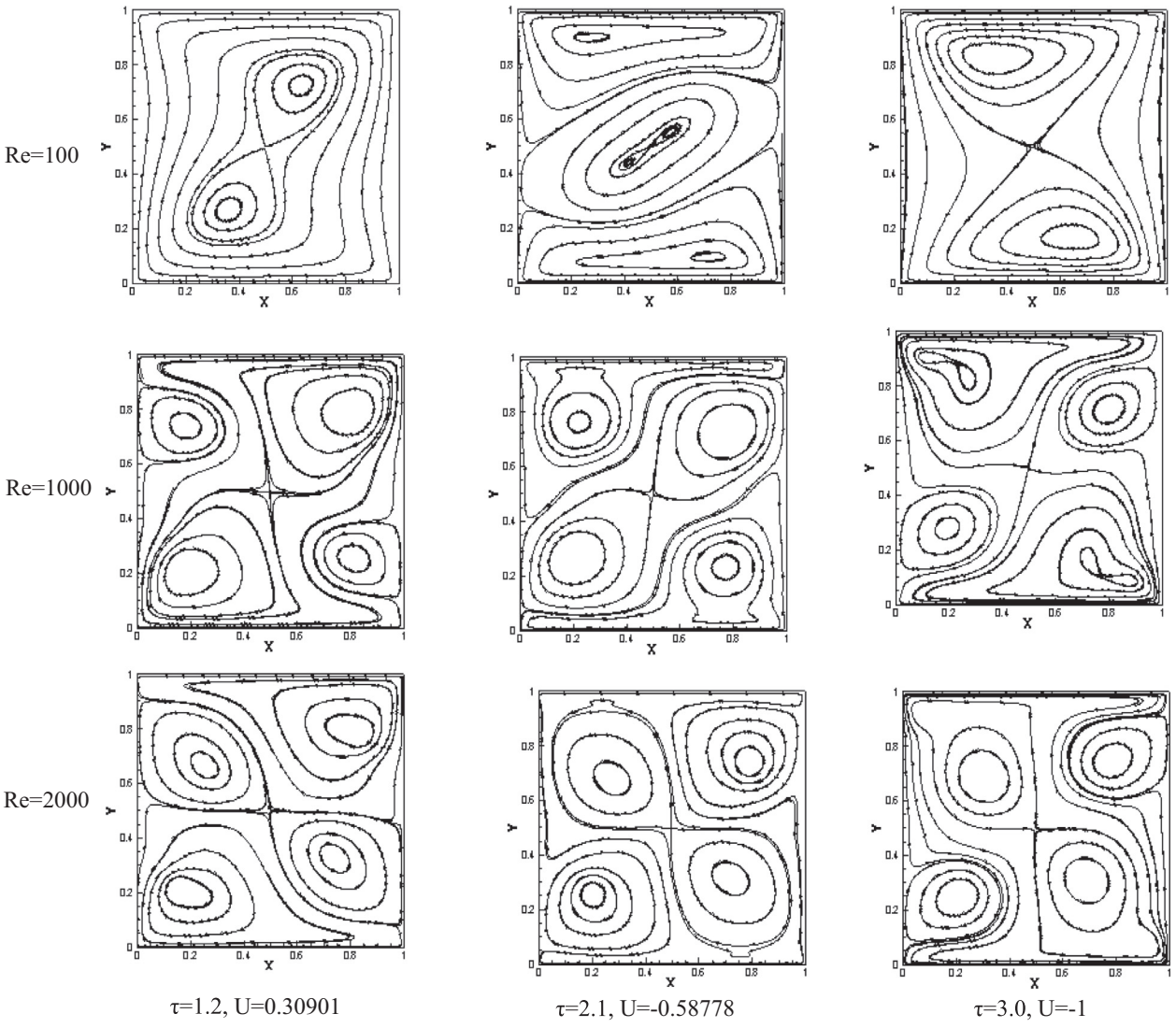

Fig. 16 Streamline patterns for anti-parallel wall oscillation at various time intervalswith optimum frequency ω = 2π/6.

for first half time interval anti-parallel wall oscillation (τ = 0–3.0). From Fig. 17(a) it is observed that the magnitude of pressure is high for low *Re* (*Re* = 100) cases and also the pressure magnitude is remaining nearly same at the starting and end of the x axis for all time intervals. The pressure magnitudes in case of anti-parallel wall oscillating case is less when compared to parallel wall oscillating case which can clearly observed from the pressure plots. As the *Re* increases (*Re* = 1000) the pressure fluctuation at the middle portion of the cavity is increasing which can be clearly observed from the plots. From Fig. 17(b) it is observed that the pressure fluctuation along y axis is more at the middle portion of the cavity for high Reynolds number (*Re* = 1000, 2000) cases.

Fig. 18 shows the vorticity gradients for the case of anti-parallel wall oscillation, from these plots it is inferred that the vorticity gradients are high when compared to the cases of single and parallel wall oscillations which means that the momentum transfer is more in the major portion of the cavity.

4. Conclusions

We develop a two-dimensional computational model to study the fluid dynamic behaviour in a oscillating lid driven square cavity using staggered grid based finite volume method with SIMPLE algorithm. Through numerical simulations, the flow behaviour and vorticity contours are analysed for three different Reynolds number (*Re* = 100, 1000 and 2000) at an optimum lid frequency. The developed numerical model is validated with the available researcher's results. The numerical simulations are carried out for the cases of single wall, parallel wall and anti-parallel wall oscillations at the optimum lid frequency. For case of parallel wall oscillations, it is found that more number of vortices are formed at *Re* = 1000, which helps in better mixing of fluid. Whereas in the case of anti-parallel wall oscillations it is observed that at *Re* = 1000 vortices are displaced by expanding and minimizing with respect to time period which indirectly indicates good mixing of fluid inside the cavity. Finally, it may be concluded that for both

Please cite this article in press as: J.V. Indukuri, R. Maniyeri, Numerical simulation of oscillating lid driven square cavity, Alexandria Eng. J. (2017), http://dx.doi.org/10.1016/j.aej.2017.07.011

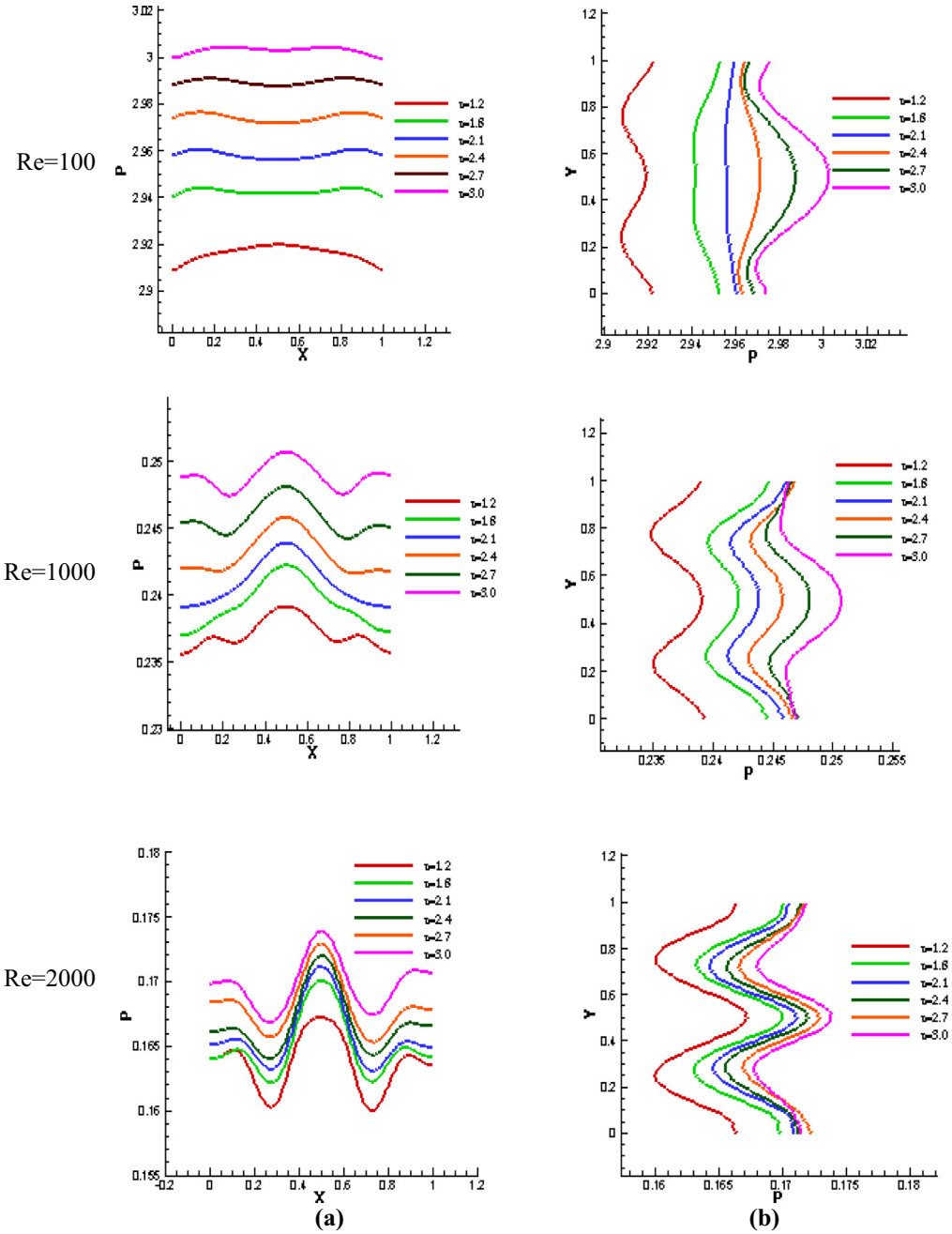

Fig. 17 Pressure distribution for anti-parallel wall oscillation at first half time interval with optimum frequency $\omega = 2\pi/6$ (a) Center line pressure variation along abscissa. (b) Center line pressure variation along ordinate.

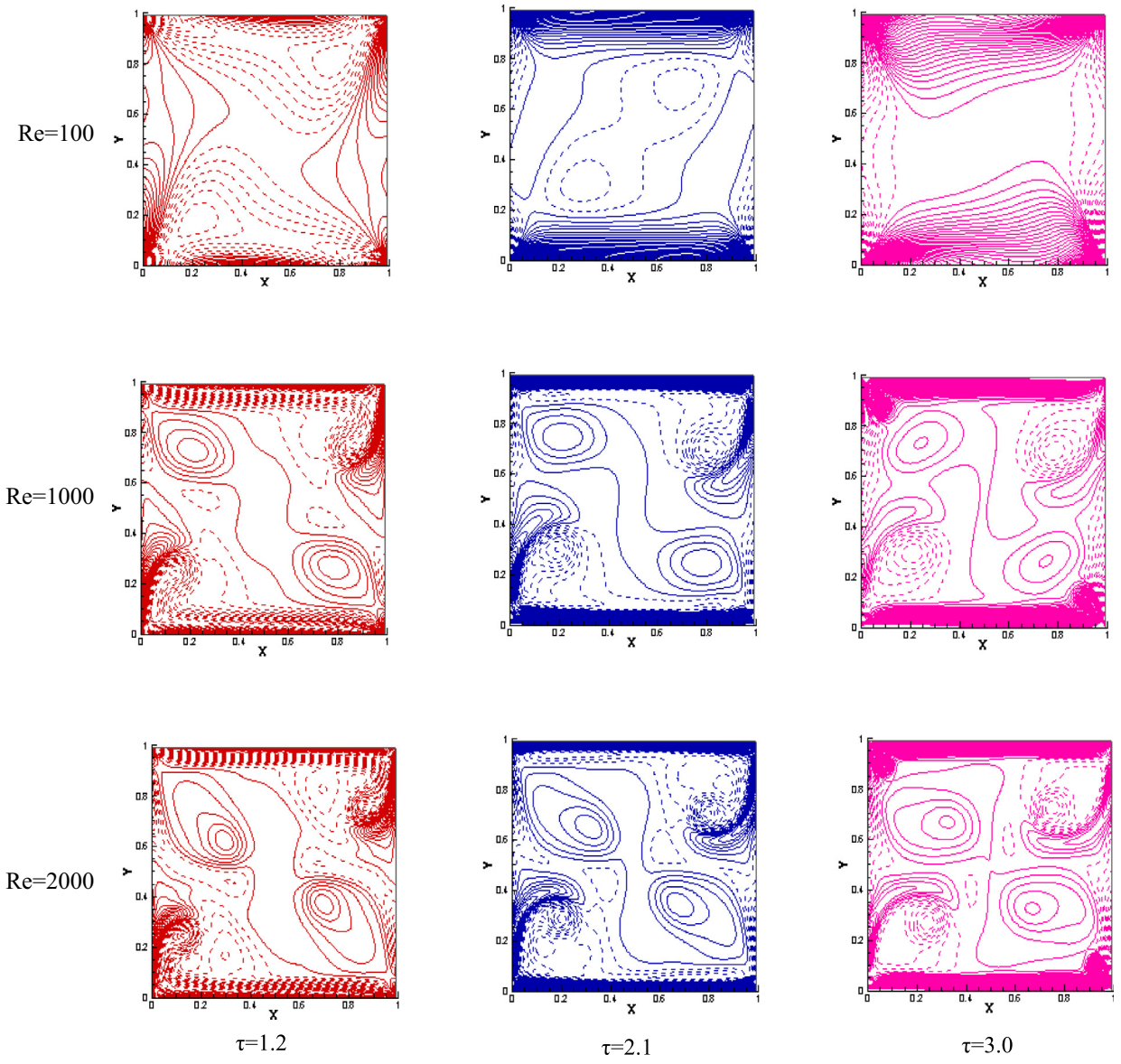

Fig. 18 Vorticity contours for anti-parallel wall oscillation at various time intervals with optimum frequency $\omega = 2\pi/6$.

the cases of parallel and anti-parallel wall oscillations better mixing of the fluid inside the cavity is observed at $Re = 1000$.

Acknowledgement

The work was supported by National Institute of Technology Karnataka, Surathkal.

References

[1] J.R. Koseff, R.L. Street, On end wall effects in a lid-driven cavity flow, J. Fluids Eng. 106 (4) (1984) 385–389.
[2] A.K. Prasad, J.R. Koseff, Reynolds number and end-wall effects on a lid-driven cavity flow, Phys. Fluids A 1 (2) (1989) 208–218.
[3] U.K.N.G. Ghia, K.N. Ghia, C.T. Shin, High-Re solutions for incompressible flow using the Navier-Stokes equations and a multigrid method, J. Comput. Phys. 48 (3) (1982) 387–411.
[4] D.V. Patil, K.N. Lakshmisha, B. Rogg, Lattice Boltzmann simulation of lid-driven flow in deep cavities, Comput. Fluids 35 (2006) 1116–1125.
[5] L.S. Lin, Y.C. Chen, C.A. Lin, Multi relaxation time lattice Boltzmann simulations of deep lid driven cavity flows at different aspect ratios, Comput. Fluids 45 (1) (2011) 233–240.
[6] D.A. Perumal, Simulation of flow in Two-Sided Lid-Driven deep cavities by finite difference method, J. Appl. Sci. Thermodyn. Fluid Mech. 6 (1) (2012) 1–6.
[7] Siva Subrahmanyam Mendu, P.K. Das, Fluid flow in a cavity driven by an oscillating lid – a simulation by lattice Boltzmann method, J. Mech. B/Fluids 39 (2013) 59–70.
[8] Hu. Zhenhong, Xing Zheng, Qing-Wei Ma, Wen-Yang Duan, Fluid flow in a cavity driven by an oscillating lid by an improved incompressible SPH, Procedia Eng. 126 (2015) 275–279.
[9] M.A. Sheremet, I. Pop, Mixed convection in a lid-driven square cavity filled by a nanofluid: Buongiorno's mathematical model, Appl. Math. Comput. 266 (2015) 792–808.
[10] N.S. Gibanov, M.A. Sheremet, H.F. Oztop, K. Al-Salem, Convective heat transfer in a lid-driven cavity with a heat-conducting solid backward step under the effect of buoyancy force, Int. J. Heat Mass Transfer 112 (2017) 158–168.
[11] S. Patankar, Numerical Heat Transfer and Fluid Flow, CRC Press, 1980.